ANNUAL STATUS REPORT

1/1/95 - 3/31/96

NASA Award NAGW-4060

Numerical Model Studies of the Martian Mesoscale circulations

M. Segal and R. W. Arritt, Principal Investigators

Agricultural Meteorology
Department of Agronomy
Iowa State University
Ames, IA 50011

1. RESEARCH OBJECTIVES

The objective of the research in the period covered in this report included the following:

(i) Studying mesoscale topographical effects on Martian flows
(ii) Further sensitivity evaluations and completion of studies initiated in previous years
(iii) Continued interaction with J. Tillman

2. ACCOMPLISHMENT

2.1 Mesoscale topographical effects on Martian Flows

a. Low level jets in the near equatorial latitudes

Previous studies indicated that western boundary currents (WBC) occur in the Martian atmosphere in the presence of large longitudinal topographical gradients, combined with β effect. It was suggested that when induced upslope flow has meridional component, it would reinforce or reduce the simulated WBC. For example, it is likely to occur in the eastern side of Syrtis (10°N) where upslope flow induced by latitudinal slope would reinforce the WBC. However, even if the slope is purely longitudinal, towards the end of the daytime and during the nighttime meridional component of the thermally induced flow resulting from inertial oscillations would reinforce or reduce the flow (depending on slope orientation and latitude). We explored these characteristics by scaling and by numerical modeling. The evaluations were carried out for various latitudes and slope inclinations.

An illustrative case in which southerly background flow of 15 $m \cdot s^{-1}$ was prescribed is described in the following. A ridge of 500 m height located at 30°N with west and east facing slopes was considered. The model results in the second day of the integration are presented. Fig. 1a presents the upslope components which are asymmetric due to adjustment of the Coriolis and frictional forces. Return circulation cells are simulated. The difference in the v component between both slopes is small (Fig. 1b). By 1800 MST intense upslope flow is simulated attributed to cessation of turbulence, while the asymmetric structure becomes more pronounced (Fig. 1c). By that time some clockwise veering of the upslope component occurred supporting the east facing slope v component and reducing in the west facing slope (Fig. 1d). From this time, inertial oscillations of the flow are almost unaffected by the thermal gradient above the elevated slopes. By 0000 MST in the slope direction shallow downslope is simulated, where lack of significant cross slope component aloft implies on completion of more than southward veering (Fig. 2a). This is supported by the respective intensification in the eastern slope v component and initiation of the strengthening of the v component in the east facing slope (Fig. 2b). Further veering of the late afternoon u component (Figs. 2c,d) resulted in continuation of this pattern by sunrise.

In the illustrated case the overshooting of the v component reached at least 7 $m \cdot s^{-1}$.

(b) Dynamical intensification of flow by steep terrain

Previous general circulation model (CCM) studies have indicated that zonally averaged surface winds on Mars are generally less than 10 m/s while zonally averaged winds aloft (above 25 kms) may easily rise to 40-80 m/s (Haberle et. al., 1993). These results are consistent with both (i) Viking lander meteorological data -- the strongest wind observed in approximately two years of time by the two probes was 31 m/s while typical values are only a few meters per second; and with (ii) Viking orbiter and Mariner data depicting cloud motions that indicate

winds of 30-55 m/s at altitudes of 15-25 kms (Leovy, 1979). These results for surface winds contrast with laboratory studies that indicate that winds of 30-60 m/s are required to raise dust (Leovy, 1979). Additional details from the GCM studies (Haberle, 1993; and Barnes, 1993) reveal that the averaged eddy kinetic energy due to planetary waves has only one fourth the kinetic energy of the mean flow, and that transient eddy winds at (or near) the surface are typically no larger than 5-20 m/s. These results indicate that typical transient surface winds (zonal mean plus planetary wave eddy component) are insufficient for raising dust into the atmosphere. This is extremely interesting because vast dust storms have been observed to occur episodically on Mars from Earth for over 100 years and more recently by spacecraft (Martin and Zurek, 1993). Possible mechanisms for generating surface winds of sufficient intensity include topographically enhanced winds; interactions between multiple cyclonic storms; and interactions between dust load, global meridional circulation, and the diurnal tide (Leovy, 1979). There is some support for the role of pre-storm atmospheric dust load based upon observations in that an increase in atmospheric opacity may be a prerequisite for the onset of a global storm. In fact the GCM studies do indicate an enhancement in mean and eddy winds when opacity increases.

We have investigated two-dimensional topographical forcing as a possible mechanism for generating surface winds sufficient to raise dust off of the surface using the gravity wave model of Prusa et. al. (1996). This model is based upon the anelastic approximation, a time variable coordinate transformation (that allows the use of transient forcing) and a highly accurate semi-Lagrangian numerical solver. Numerical solutions for two fundamentally different cases were generated:

Case M1. Flow over a high (5.0 km) mountain ridge
Case M2. Flow over a more moderate (1.5 km) and broader ridge.

The basic state atmosphere in each case was given a scale height of 11.0 kms and a surface wind of 15 kms. The zonal wind inceased with height with constant shear until it reached 50 m/s at a height of 40 kms, from which point it was uniform to the top of the computational domain. This basic state is a rough approximation to the zonal mean state of the atmosphere at equatorial to southern sub-tropical latitudes during southern summer solstice conditions (Haberle, 1993) -- the time and locations most favored for dust storms (Martin and Zurek, 1993). The numerical model allows the use of two types of initial conditions: (i) an initial state in which there is no perturbation to the basic state and the mountain is slowly "grown" to its full height; and (ii) a potential flow initial condition about the full topographical disturbance. Case M1 was run using both types of initial condition, and while there were significant differences in the initial evolution of the mountain wave field, the long term behavior was very similar showing that it was a very robust feature of the flow.

Results for case M1 are shown in Figures 3 and 4. Fig. 3 shows the nonlinear development of the potential temperature field. The basic state is one of constant stability with a potential temperature scale height of 90.0 kms, corresponding to a Brunt-Vaisala frequency of 0.0064/s. The initial condition used was a potential flow over the full height topography - a gaussian mountain with a peak half width of 50 kms. Two hours after the onset of forcing (Fig. 3a), vigorous wave breaking has begun 20 kms downsream from the peak and some 55 kms above it. Just above the downslope flank of the mountain, waves are becoming saturated. At 180 minutes (Fig. 3b) an extended region of vigorous breaking has developed at higher altitudes, while waves on the downslope flank are breaking 40 to 80 kms from the peak. As time increases to 210 (Fig. 3c) and finally 240 minutes (Fig. 3d), the breaking region on the downslope flank grows in extent, ultimately to well over 120 kms in length. The flow field is highly unsteady, and consists of vortices forming over the peak and being shed downstream. It is very similar to

downslope windstorms known to occur on Earth (Klemp and Lilly, 1977; Clark and Peltier, 1984). Such storms can easily accelerate mean winds by 50% or more compared to the intial state over an extended region. Our results for zonal wind bear this out. Fig. 4 shows the zonal wind field from 120 to 240 minutes after the onset of forcing. At 120 minutes (Fig. 4a), wave breaking has resulted in the local depostion of momentum (via Eliassen-Palm flux divergence) such that in the wave breaking region, local winds below -20 and above +100 m/s occur. Departures from the background wind are thus the same order of magnitude as the background wind itself. Near the surface, the winds are much less extreme, but above 40 m/s from the peak to 80 kms downslope. At 180 minutes (Fig. 4b), again surface winds are over 40 m/s for an extended range (from the peak to 90 kms downslope). But now a very localized region (one grid cell) appears with peak winds over 60 m/s just over 60 kms downslope from the peak. By 210 minutes (Fig. 4c), three localized regions appear that have peak surface winds in excess of 60 m/s, at 19, 38, and 58 kms downslope. They range in length from 5 kms (the first -- which actually lies a few kilometers above the surface) to about 10 kms. Very similar features are seen at 240 minutes (Fig. 4d). Several high wind gusts (over 60 m/s) appear at 20, 55, and 99 kms downslope from the peak. These localized regions of high winds move downslope and utimately lose intensity while new gusts are generated near the peak which then move downstream.

Case M2, not shown here, exhibited strikingly different behaviour. It evolved into a steady state solution without significantly modifiying the initial potential flow field. Only a very weak, linear wavefield developed which failed to become nonlinear (let alone break) even after 10 hours of integration. Although we are still investigating the physical reasons behind this, Froude number similarity may be a major factor. The Froude number is defined as Fr = u/(A * N), where u is the zonal wind, A the amplitude of the topographical disturbance, and N the Brunt-Vaisala frequency. Based upon the basic state surface wind, Fr is 0.47 for case M1 and 1.04 for case M2. For Fr << 1, breaking should occur very near the mountain, whereas for Fr >>1, breaking should occur aloft (Smolarkiewicz and Rotunno, 1989). Given these values of Fr number, it is interesting to note that in both cases that breaking begins aloft. Evidently the Froud number based upon the zonal wind aloft is more important for determining the location of initial wavebreaking. This Froude number has values of 1.56 and 3.47 for cases M1 and M2, respectively, that correspond well with the altitudes of waves that first break. For the development of downslope windstorms in particular, the Froude number (for uniform basic state zonal wind) must be less than 1.18 (Clark and Peltier, 1984). It is thus somewhat surprizing that only case M1 developed a windstorm. Possibly the resonant growth of trapped modes also needs to be considered (Clark and Peltier, 1984; Keller, 1993). Since the basic state zonal wind has shear, it acts as a filter -- trapping waves with group velocities equal to the local wind. However, a preliminary analysis using a quasi-stationary approximation (Prusa et. al., 1996) reveals that trapped internal waves in case M2 are more likely to resonate that those in case M1. It is possible that unsteady waves for which the quasi-stationary approximation is not valid play a fundamental role.

Additional future investigations should be done to illuminate the physical reasons that case M2 did not develop a windstorm. Although 5 km topography does ocurr on Mars, the gentler topography of case M2 is much more common, with candidate features for downslope windstorms identifiable on the Atlas of Mars Topographic map (eg. Viking 2 orbiter photos clearly show a nascent dust storm located SW of Claritas Fossae centered at 42.5 S latitude and 108 W longitude. The storm appears roughly aligned with Claritas Fossae which could possibly have provided topographical forcing if the winds were from the NE).

2.2 Further sensitivity evaluations and completion of studies initiated in previous

years.

(i) The study evaluating the dissipation of cold air mass outbreaks due to enhanced sensible heat flux was completed and a paper was submitted to *J. Atmos. Sci.*

(ii) Further sensitivity and scaling evaluations were carried out for generalization of the characteristics of Martian mesoscale circulations caused by horizontal sensible heat-flux gradients.

(iii) In conclusion of the previous year evaluations of rocks' impact on boundary layer processes, evaluations were carried out on the significance that non-uniform surface would have on enhancing the polar CO_2 ice sublimation during spring. Utilizing the soil heat conduction equation, evaluations were made to explore the impact of horizontal conduction of heat from small patches of CO_2 ice free surfaces (e.g. because of small area exposed rock) to the CO_2 ice covered soil. For spring solar conditions, it was found that such heat conduction has a larger impact on sublimation at the *edge* of the CO_2 ice cover than solar irradiance. It was concluded that when the CO_2 ice layer is thin, the integrated effect on CO_2 ice sublimation by this process is significant.

2.3 Interaction with Jim Tillman

Jim Tillman analyzed the Viking Lander VL-2 maximum temperature (T_{max}), minimum temperature (T_{min}) and daily mean temperature (T_{mean}; based on diurnal averaging). He found that during the period summer-fall, the T_{max} were consistently higher by ~ 5 K during the period summer-fall of the second year, whereas the corresponding T_{min} and T_{mean} values resembled those of the first year. In order to explore the reasons for these patterns, numerical modeling sensitivity simulations were carried out. Multiple 1-D model simulations were carried out while generating composites of response of T_{max} and T_{min} to variation of the various relevant parameters as described in the following:

(a). Sensitivity to change in wind speed

Composite of the temperature at 1.6 m at 1500 MST (when about the daily maximum temperature is obtained), were generated for various wind speed and latitudes (Fig. 5a). T_{max} was found to increase about linearly with the wind speed. On the other hand at 0300 MST (when about the daily minimum temperature is obtained) no dependency on wind speed is simulated (Fig. 5b)

b. Additional effects

Additional sensitivity simulations were carried out to evaluate the impact of small changes in surface albedo (Figs.5c,d), and deep soil temperature on T_{max} and T_{min}. These were found to be secondary to these obtained in (a) above. Tentatively it is suggested that change in wind speed climatology between both years provides partial support to the observational features found by Tillman. Presently the potential impact of subsidence due to dynamical causes are evaluated.

2.4 References

Barnes, J.R., Pollack, J.B., Haberle, R.M., C.B. Leovy, and R.W. Zurek. 1993. Mars Atmospheric Dynamics as simulated by the NASA Ames General Circulation Model 2. Transient Baroclinic Eddies. *J. Geophysical Research*, **98**, 3125-3148.

Clark, T.L. and W.R. Peltier. 1984. Critical Level Reflection and the Resonant Growth of Nonlinear Mountain Waves. *J. Atmospheric Sciences*, **41**, 3122-3134.

Haberle, R.M., Pollack, J.B., Barnes, J.R., and R.W. Zurek. 1993. Mars Atmospheric Dynamics as simulated by the NASA Ames General Circulation Model 1. The Zonal-Mean Circulation. *J. Geophysical Research*, **98**, 3093-3123.

Keller, T.L. 1993. Implications of the Hydrostatic Assumption on Atmospheric Gravity Waves. *J. Atmospheric Sciences*, **51**, 1915-1929.

Klemp, J.B. and D.K. Lilly. 1977. Numerical Simulation of Hydrostatic Mountain Waves. *J. Atmospheric Sciences*, **35**, 78-107.

Leovy, C.B. 1979. Martian Meterorology. *Annual Review Astronomy and Astrophysics*, **17**, 387-413.

Martin, L.J. and R.W. Zurek. 1993. An Analysis of the History of Dust Activity on Mars. *J. Geophysical Research*, **98**, 3221-3246.

Prusa, J.M., Smolarkiewicz, P.K., and R.R. Garcia. 1996. On the Propagation and Breaking at High Altitudes of Gravity Waves Excited by Tropospheric Forcing. To be published in the J. Atmospheric Sciences.

P.K. Smolarkiewicz and R. Rotunno. 1989. Low Froude Number Flow Past Three-Dimensional Obstacles. Part I: Baroclinically Generated Lee Vortices. *J. Atmospheric Sciences*, **46**, 1154-1164.

3. OBJECTIVES FOR THE LAST YEAR OF THE AWARD (4/1/96 - 4/1/97)

In the last year of the award we will focus on final sensitivity evaluations and on preparing documentation of the studies carried out in the previous period of the award. These include the following:

i) Martian mesoscale circulations caused by horizontal sensible heat flux gradient
ii) Dynamical impact of mesoscale topography on Martian flows.
iii) Martian surface characteristics' impact on boundary layer growth.

4. PUBLICATIONS SUPPORTED BY GRANT NAGW-4060

Segal, M. (1994): Mesoscale meteorology patterns in the proposed Pathfinder landing sites In: Notes and handouts from the second Mars Pathfinder Project Science Group Meeting 9-10 June, JPL Pasadena, CA.

Tillman, J., D. R. Sandstrom, S. Larsen and M. Segal (1994): Martian planetary boundary layer/climatology station. In Mars Surveyor Science Objectives and Measurements Requirements Workshop. May 10-12, JPL, Pasadena, CA, 162-163.

Prusa, J., P. K. Smolarkiewicz, and R. R. Garcia (1996): Gravity Wave Breaking Near the Mesopause, *J. Atmos. Sci.* (accepted).

Segal, M., R. W. Arritt, and J. Tillman, 1996: On the potential impact of daytime surface sensible heat flux on the dissipation of Martian cold air outbreaks (submitted to *J. Atmospheric Science*).

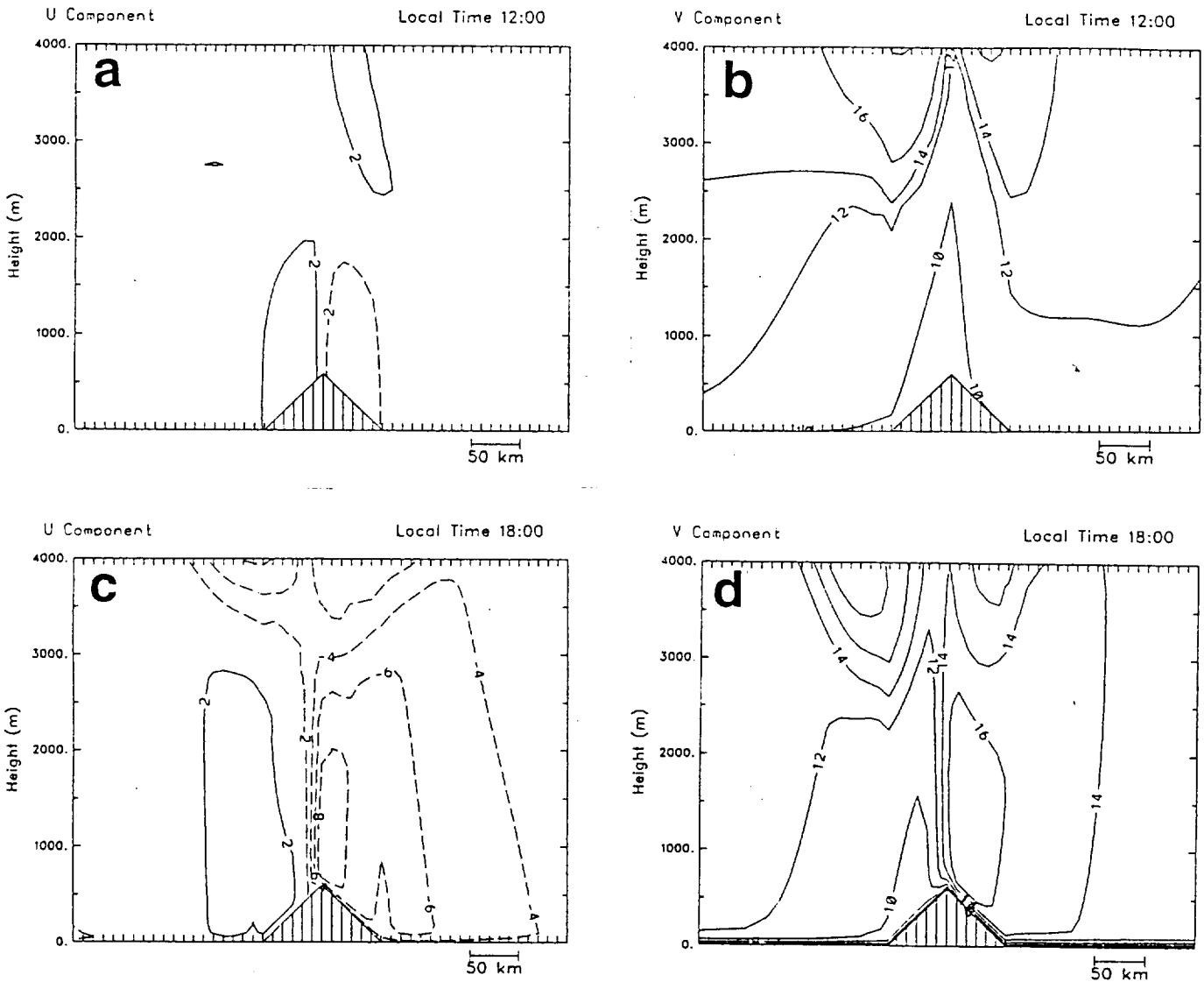
U Component
Local Time 12:00
a
Height (m)
4000.
3000.
2000.
1000.
0.
50 km
V Component
Local Time 12:00
b
U Component
Local Time 18:00
c
V Component
Local Time 18:00
d

Fig. 1

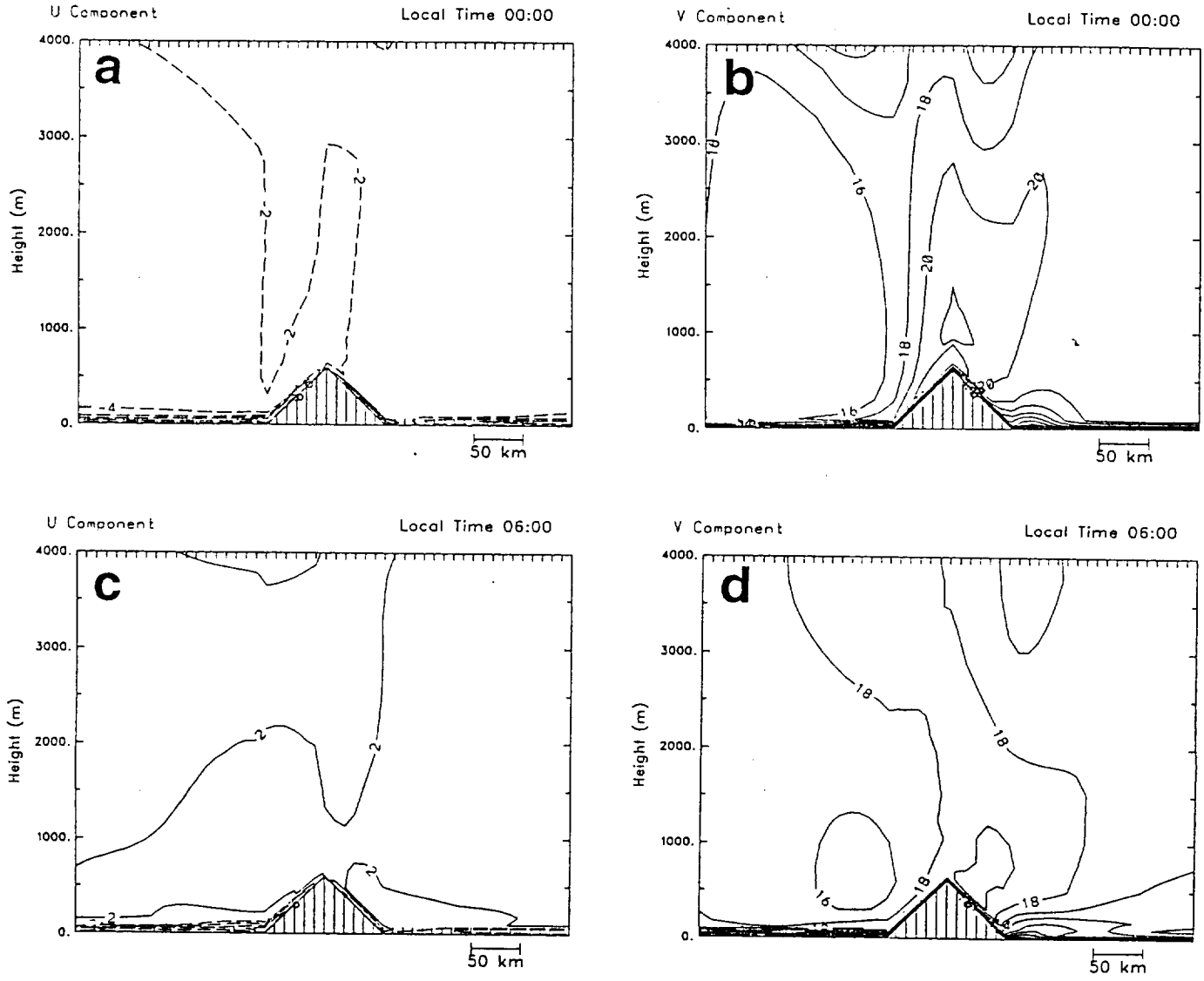
U Component
Local Time 00:00
a
Height (m)
4000.
3000.
2000.
1000.
0.
-2
-4
50 km
V Component
Local Time 00:00
b
16
18
20
50 km
U Component
Local Time 06:00
c
2
50 km
V Component
Local Time 06:00
d
16
18
50 km

Fig. 2

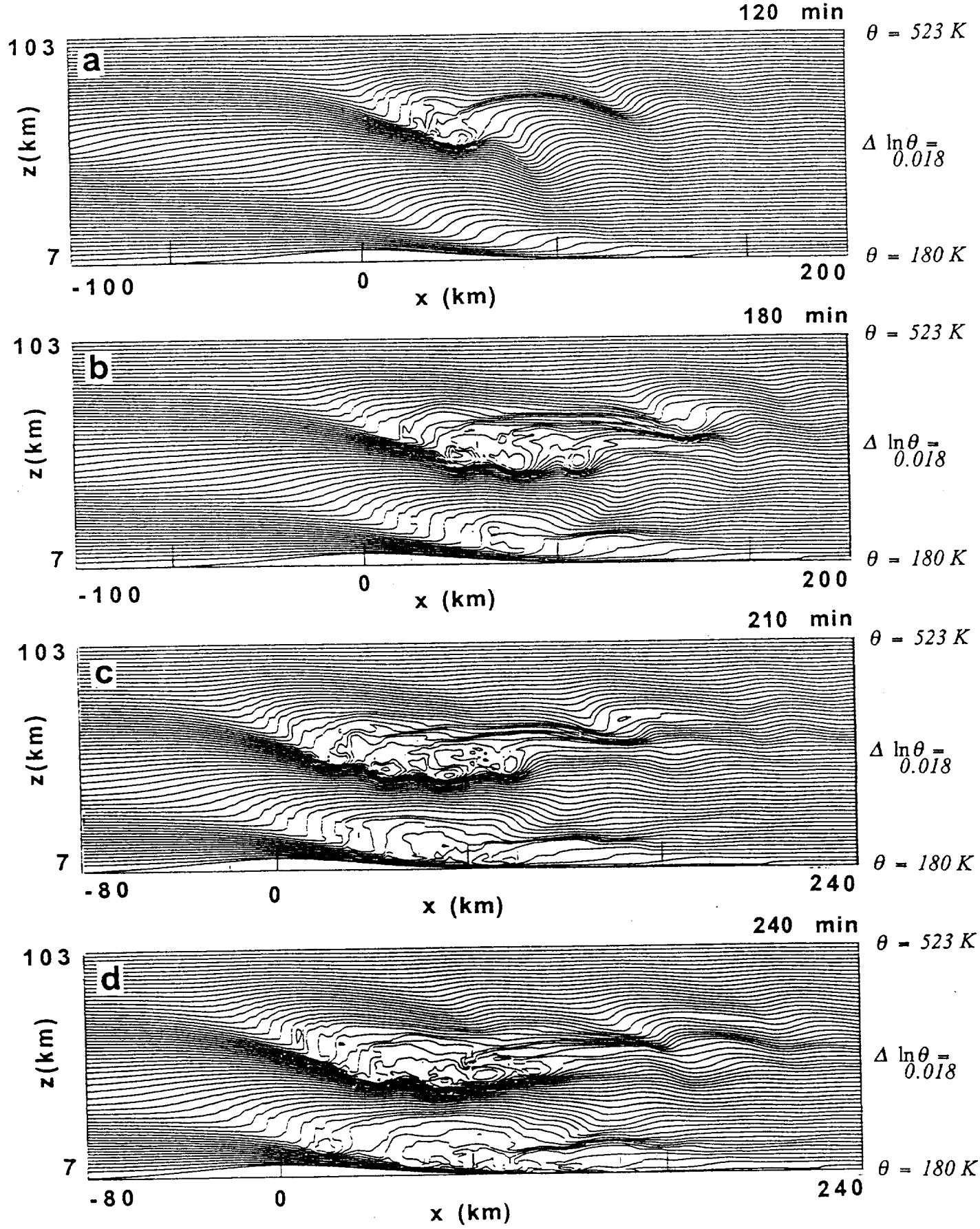
120 min
103
a
z(km)
7
-100
0
200
x (km)
θ = 523 K
Δ ln θ = 0.018
θ = 180 K
180 min
103
b
z(km)
7
-100
0
200
x (km)
θ = 523 K
Δ ln θ = 0.018
θ = 180 K
210 min
103
c
z(km)
7
-80
0
240
x (km)
θ = 523 K
Δ ln θ = 0.018
θ = 180 K
240 min
103
d
z(km)
7
-80
0
240
x (km)
θ = 523 K
Δ ln θ = 0.018
θ = 180 K

Fig. 3

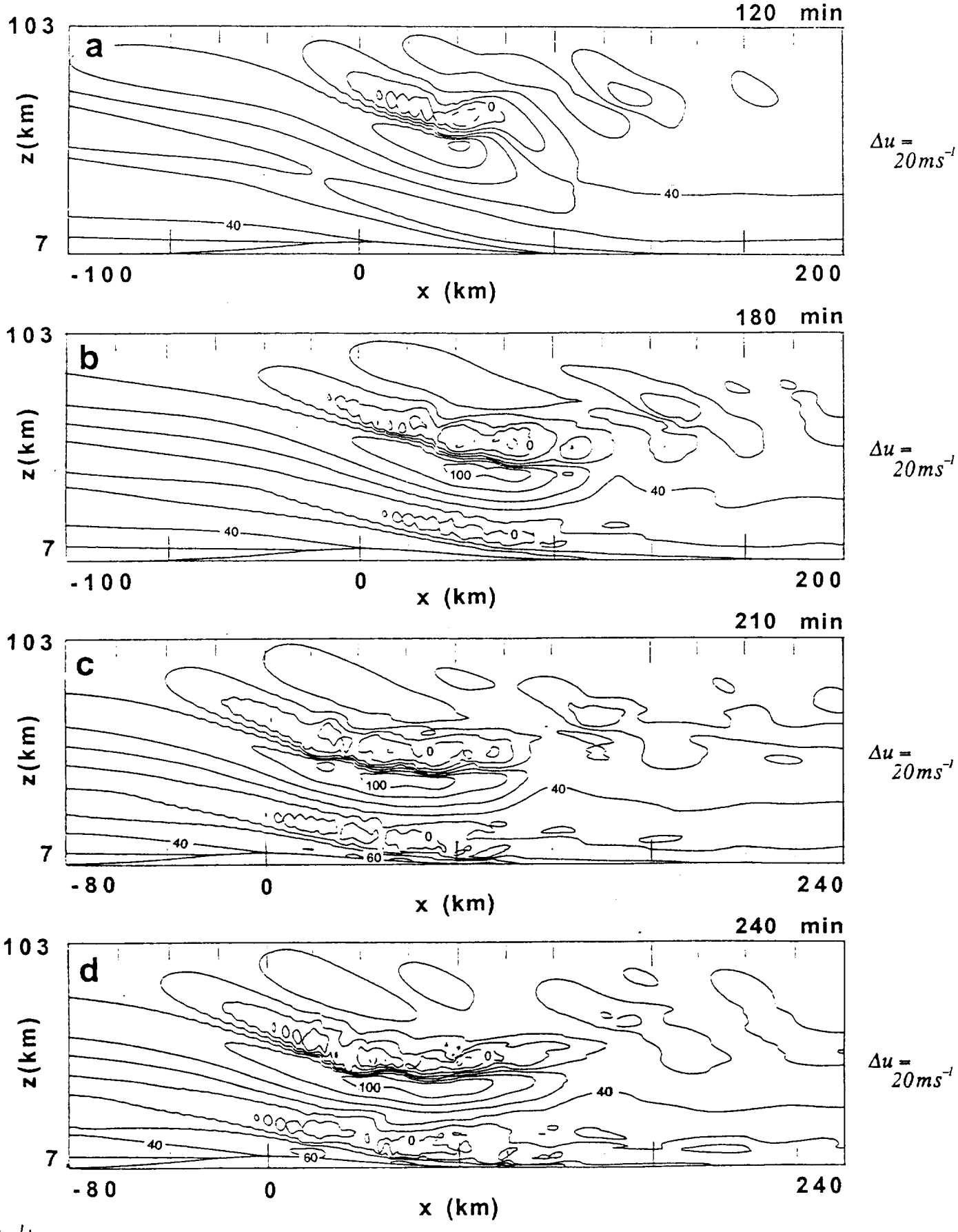
120 min
a
103
z(km)
7
-100
0
200
x (km)
0
40
40
Δu = 20ms⁻¹
180 min
b
103
z(km)
7
-100
0
200
x (km)
0
100
40
40
0
Δu = 20ms⁻¹
210 min
c
103
z(km)
7
-80
0
240
x (km)
0
100
40
40
0
60
Δu = 20ms⁻¹
240 min
d
103
z(km)
7
-80
0
240
x (km)
0
100
40
40
0
60
Δu = 20ms⁻¹

Fig. 4

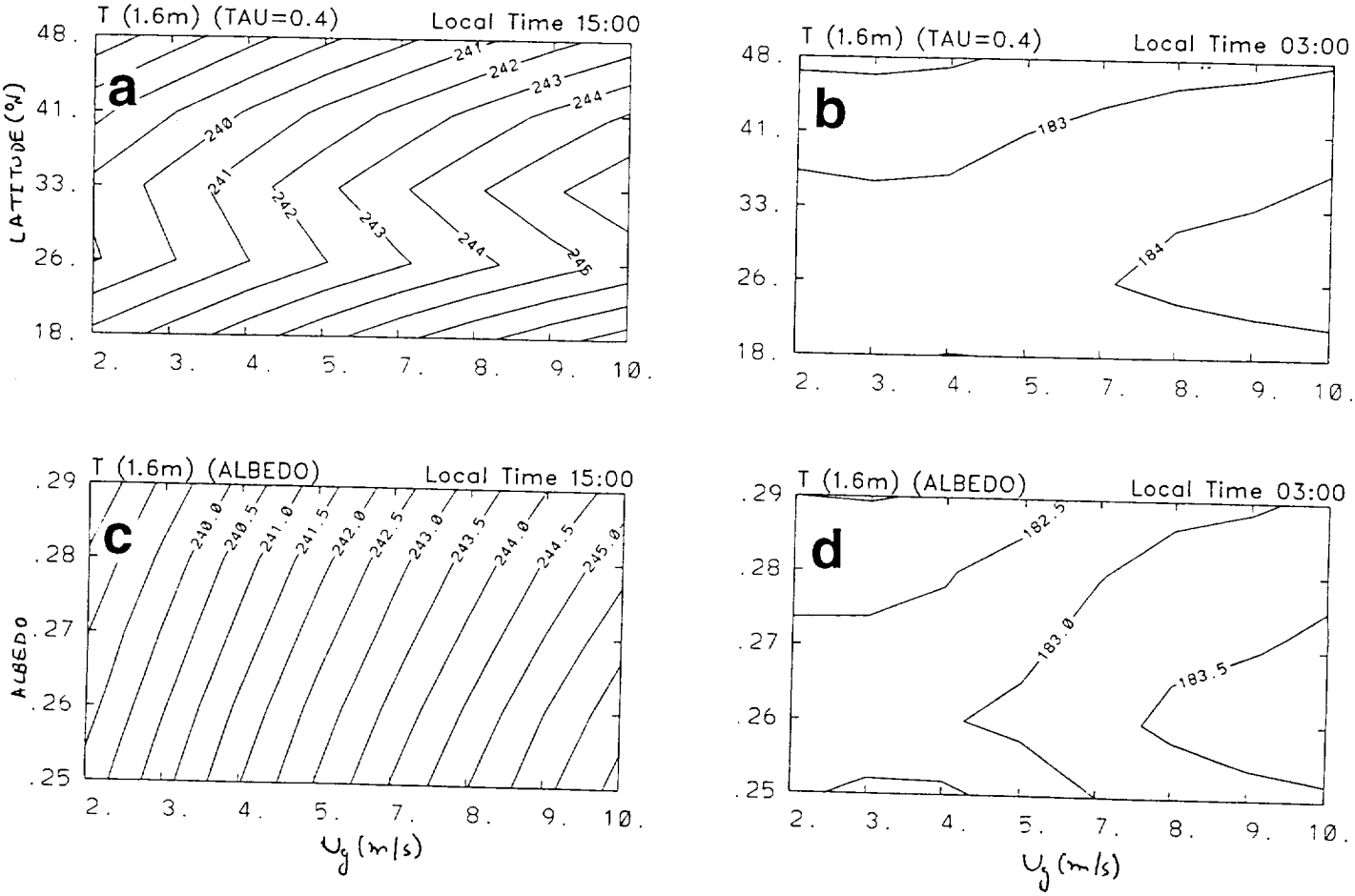
T (1.6m) (TAU=0.4)
Local Time 15:00
a
LATITUDE (N)
48.
41.
33.
26.
18.
2. 3. 4. 5. 7. 8. 9. 10.
240
241
242
243
244
245
T (1.6m) (TAU=0.4)
Local Time 03:00
b
183
184
T (1.6m) (ALBEDO)
Local Time 15:00
c
ALBEDO
.29
.28
.27
.26
.25
240.0
240.5
241.0
241.5
242.0
242.5
243.0
243.5
244.0
244.5
245.0
Ug (m/s)
T (1.6m) (ALBEDO)
Local Time 03:00
d
182.5
183.0
183.5
Ug (m/s)

Fig. 5